한국수소 및 신에너지학회 논문집(2006.6), 제17권 제2호
Trans. of the Korean Hydrogen and New Energy Society (2006.6), Vol. 17, No. 2, pp. 193~203

고속 헬륨 제트 유동의 실험적 분석을 위한 4차원 디지털 스펙클 토모그래피 기법 개발

고한서*†, 김용재*
*성균관대학교 기계공학부

Development Of Four-Dimensional Digital Speckle Tomography For Experimental Analysis Of High-Speed Helium Jet Flow

Han Seo Ko*† and Yong-Jae Kim*
**School of Mechanical Engineering, Sungkyunkwan University 300 ChunChun-Dong, JangAn-Gu, Suwon, KyungGi-Do 440-746 Korea*

ABSTRACT

A high-speed and initial helium jet flow has been analyzed by a developed four-dimensional digital speckle tomography. Multiple high-speed cameras have been used to capture movements of speckles in multiple angles of view simultaneously because a shape of a nozzle for the jet flow is asymmetric and the initial jet flow is fast and unsteady. The speckle movements between no flow and helium jet flow from the asymmetric nozzle controlled by a solenoid valve have been obtained by a cross-correlation tracking method so that those distances can be transferred to deflection angles of laser rays for density gradients. The four-dimensional density fields for the high-speed helium jet flow have been reconstructed from the deflection angles by a developed real-time tomography method.

KEY WORDS : Digital Speckle Tomography(디지털 스펙클 토모그래피),Hydrogen Flow(수소 유동), High-speed Helium Flow(고속 헬륨 유동), Multiplicative Algebraic Reconstruction Technique (MART)(곱셈산술재건법), Cross-correlation(상호 상관법)

1. Introduction

Hydrogen is the most important future energy to decrease the green house effect and to increase the efficiency of the energy consumption. Since hydrogen is very light and has very big

†Corresponding author: hanseoko@yurim.skku.ac.kr

combustibility, a leakage of the hydrogen in a room is very dangerous[1]. Thus, the four-dimensional digital speckle tomography has been developed in this study to investigate the hydrogen gas flows during a leakage for a safety system. The high-speed and initial helium jet flow has been analyzed since the behavior of the hydrogen gas flow is very similar to that of the helium flow.

Deflection angles of projected beam can be recorded by a laser speckle photography nonintrusively since refractive index variation of a phase object deflects the incident laser beam[2]. Using the Gladstone-Dale relation[3], the deflection angle a can be given as a ray integral of the field density gradient:

$$\psi_{SP}(s,\theta) \cong \alpha = G\int \frac{\partial \rho}{\partial s} dt \tag{1}$$

where y_{SP} is the projection of the digital speckle analysis, s is perpendicular to, t is parallel to the incident ray, and G is the Gladstone-Dale constant. The digitally recorded specklegrams have been evaluated numerically by a cross-correlation method instead of interrogating a double-exposed photographic film by a second laser for the speckle photography[4]. The reconstructed densities are the relative helium densities in the mixture of helium and air as follows:

$$\rho^* = \frac{\rho_{air} - \rho}{\rho_{air} - \rho_{helium}} = \frac{\rho_h}{\rho_{helium}} = \frac{n_{air} - n}{n_{air} - n_{helium}} \tag{2}$$

where r^*, r_{air}, r_{helium}, and r_h are, respectively, the relative helium density in the mixture of helium and air, ambient air density, pure helium density, and the partial density of helium in the mixture, and n_{air}, n_{helium}, and n are the refractive indices of ambient air, pure helium, and the mixture of helium and air in the jet at atmospheric pressure and room temperature, respectively. Thus, the limiting values of r^* are $r^* = 1$ for pure helium and $r^* = 0$ for pure air[5]. The deflection angle, in Eq. (1) must be inverted to reconstruct the true density field, $r(x,y,z)$ by the speckle tomography[6]. Since the tomography methods such as the algebraic reconstruction technique (ART)[7] and multiplicative algebraic reconstructiontechnique (MART)[8] update the density distributions by using the feedback information of the density itself instead of the density gradient, the ray deflection angle Y_{SP} from the digital speckle system should be converted to the interferometric fringe shift Y_{IF} which can be expressed as the integration of the density itself as follows[9]:

$$\psi_{IF} = \frac{G}{\lambda}\int(\rho - \rho_{ref})dt = \frac{1}{\lambda}\int(n - n_{ref})dt \tag{3}$$

where l, r_{ref}, and n_{ref} denote the wave length of a laser ray, the reference density, and the reference index of tefraction, respectively. The Mach-Zehnder interferometer directly measures the fringe shift to calculate the refractive index by the tomographic reconstruction algorithm for asymmetric flow cases and the absolute density values can be calculated from Eq. (2). The finite fringe shift for the interferometry can be measured by the number of fringe crossings at any point of the viewing screen as compared to the reference fringes. The deflection angle Y_{SP} can be determined for any point of the field of view

from a measurement of the displacement of the respective light ray in the recording plane while the wave front interferometry creates the path length difference between the reference beam and the test beam that goes through a phase object. The resulting fringes Y_{IF} are then shifted with respect to the undisturbed fringes which are formed by the two beams without a tested phase object. Note that the fringe shift number is determined directly by the ray integration of the density field, whereas the beam deflection angle of the digital speckle system is given by the ray integration of the density gradient. Thus, the relation between the measurements of the digital speckle system and the interferometry can be derived from the differentiation of the fringe shift along the perpendicular direction of the light ray s. Combining Eqs. (1) and (3) gives

$$\frac{\partial \psi_{IF}}{\partial s} = \frac{G}{\lambda}\frac{\partial}{\partial s}\int(\rho - \rho_{ref})dt = \frac{G}{\lambda}\int\frac{\partial \rho}{\partial s}dt = \frac{1}{\lambda}\psi_{SP} \tag{4}$$

where s is perpendicular to and t is parallel to the incident light ray. Integrating Eq. (4) along the direction s on the projection plane gives

$$\psi_{IF} = \frac{1}{\lambda}\int \psi_{SP}\, ds \tag{5}$$

Equation (5) implies that an integral of the ray deflection angle, y_{SP}, along s is equivalent to the interferometric fringe shift number y_{IF}. Once this modification is made, the feedback information of the ART and the MART will carry the index of refraction discrepancies instead of the index of refraction gradient discrepancies for the digital speckle system to obtain the density values by Eq. (2).

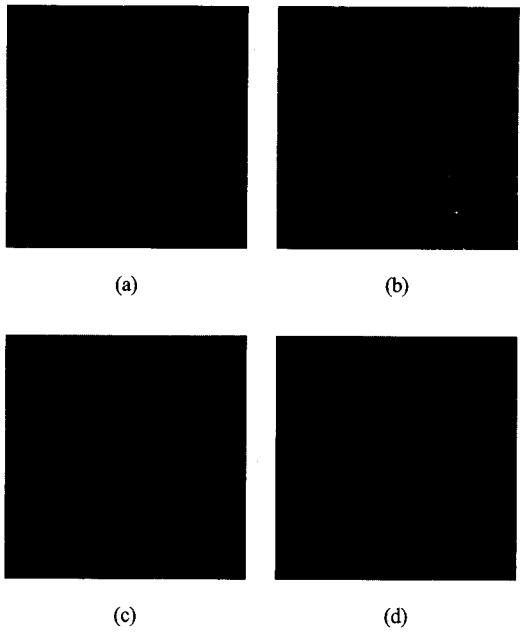

Fig. 1 Digital speckle images of high-speed helium jetflow for three projection angles of view (P = 2.5 bar), (a) no flow, (b) projection 1 (60°), (c) projection 2 (0°), and (d) projection 3 (-90°)

The objective of this study is to reconstruct the transient and asymmetric density distributions for a high-speed helium jet flow using the four-dimensional digital speckle tomography from the simultaneous and instantaneous speckle-displacement measurements by the cross-correlation method. Thus, the specklegram images have been captured by three high-speed cameras and an image capturing board simultaneously for three projection angles of view before the reconstruction.

2. Digital Speckle Analysis

The digital speckle method just records the original speckle image and the dislocated speckle images separately using three high-speed cameras as shown by Figs. 1 (a) to (d) for the initial helium jet flow. One of the purposes of this study

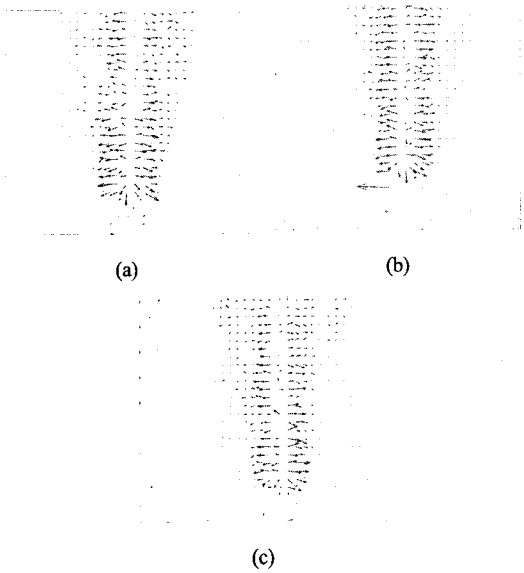

Fig. 2 Speckle displacements by cross-correlation method for speed helium jet flow, (a) projection 1 (60°), (b) projection 2 (0°), and (c) projection 3 (-90°)

is to develop a new three-dimensional reconstruction technique to obtain the accurate density distribution using limited number of projection angles for a real engineering field because the reconstruction of practical problem is viable in limited and restricted projections to a degree due to spatial and other restrictions.

Therefore, three projection angles have been tested in this study. The speckle movements are calculated by the cross-correlation method[10] like a particle tracking method of a particle image velocimetry (PIV).

For the cross-correlation method, rectangular interrogation areas have been developed instead of square ones because most of the speckles in this study move horizontally as shown in Figs. 2 (a) to (c) for the upward helium jet flow in three projection angles of view. There is no speckle displacement outside the beam area and the nozzle position in Fig. 2. The speckle dislocations caused by the beam deflection angle are expressed as the lines to identify the directions while the dots indicate no speckle displacement in Fig. 2. From the simultaneous and instantaneous measurements of the speckle dislocations using three projection angles of view, the deflection angles can be calculated as follows:

$$\alpha \equiv \tan \alpha = \frac{\delta}{l} \tag{6}$$

where d is the speckle displacement and l is the distance between a test section and a viewing screen. The transient and asymmetric density distributions can be reconstructed by the tomography method after the deflection angle Y_{SP} is converted to the interferometric fringe shift Y_{IF} by Eq. (5).

3. Tomographic Reconstruction Algorithm : Multiplicative Algebraic Reconstruction Technique (MART)

The deflection angle, in Eq. (1) must be inverted to reconstruct the true density field, $r(x,y,z)$ by the speckle tomography. The tomographyundertakes the optimization task for the linear case where each basis function is defined by a single parameter (its unknown height with a fixed spread). The location of each three-dimensional basis function is given as

$$\hat{f}(x,y,z) = \sum_{j=1}^{JKL} O_j b(x-x_j, y-y_j, z-z_j) \tag{7}$$

where $\hat{f}$ is an object function that represents the field to be reconstructed, b is a general form of the basis function located at (x_j,y_j,z_j), and O_j is the height coefficient of the j-th basis function centered at a fixed location of (x_j,y_j,z_j). The (x_j,y_j,z_j) positions form a hexadral array of J, K

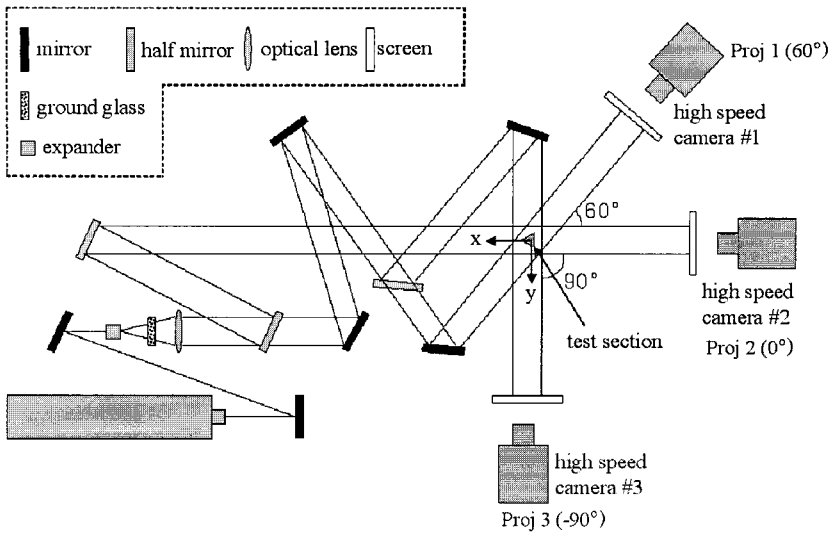

Fig. 3. Schematic diagram of digital speckle system for high-speed helium jet flow

and L equally spaced points in the x, y and z directions, respectively. Thus, $J\times K\times L$ is the total number of coefficients to be estimated by the reconstruction algorithm. The use of a smooth basis function such as the cubic B-spline function[11] can accurately represent a relatively smooth object field with far fewer coefficients than with the square-pixel basis function. An optimized set of these unknowns must be found to minimize the deviations between the virtual projection $\hat{\psi}$ of an intermediate object function $\hat{f}$ and the measured projection y of the actual field f. The developed four-dimensional tomography including variation of time in this study reconstructs the four-dimensional density field simultaneously instead of piling up the cross-sectional density distributions with time because the real-time and three-dimensional objection function has been expressed by Eq. (7). The multiplicative algebraic reconstruction technique (MART) uses an element C_j of the multiplicative correction vector C as follows[9]:

$$O_j^{q+1} = C_j^q O_j^q$$

$$C_j^q = \begin{cases} 1 - 0.5W_{i,j}\left(1 - \dfrac{\psi_i}{\hat{\psi}_i}\right), & \hat{\psi}_i \neq 0 \\ 1, & \text{otherwise} \end{cases} \tag{8}$$

where q denotes the q-th iteration and the normalized weighting factor $W_{i,j}$ is equal to $w_{i,j}/w_{max}$ where w_{max} is the largest element of the projection matrix W. The MART ensures a non-negative object field in reconstructing non-negative scalar. Note that the algorithm update is possible only for algebraic projections in which the ray integration of the field directly gives the projection data, such as in interferometry (Eq. (3)). Therefore, for the digital specklegram the ray sum must be changed from y_{SP} to y_{IF} by Eq. (5) and then the MART can be used to calculate the four-dimensional density distributions simultaneously. Although the digital speckle

analysis requires one more step for integrating the deflection angles to calculate the interferometricprojections, the results of the digital specklegram give a smooth density distribution and acceptable accuracy because lots of the speckles are used to measure the deflection angles for the tomography.

4. Experimental Setup

The density distribution of the unsteady and high-speed helium jet flow from a triangular nozzle has been observed by a continuous-wave Nd:YAG laser using the four-dimensional digital speckle tomography. The nozzle is made of copper and the length of one side for a regular triangle is 8 mm. The laser beam is expanded by a 10X beam expander and directed at an optical lens via a ground glass as shown by Fig. 3. The camera lens has the focal length of 50mm and the pixel resolution of 256 × 256 pixels with f/1.8 and the effective speckle size of the ground glass is about 1mm on the viewing screen.

After opening the helium tank at 2.5 bar and the solenoid valve for the high-speed helium jet flow perpendicular to the laser beam, the images of the initial helium jet flow have been captured for 1 second with the interval of 1/15000 sec by three high-speed cameras. For the experiment, the specklegram images have been recorded in three different angles of view simultaneously because the initial helium jet flow is asymmetric and unsteady. From those three specklegram images, the speckle displacements have been calculated by the cross-correlation method. And then, the three-dimensional and transient density distributions have been reconstructed by the developed real-time four-dimensional MART in this study.

5. Results and Discussion

The four-dimensional density distribution at Reynolds number of 6400 has been reconstructed from 2 mm to 26 mm above the nozzle after calculating the speckle displacements by the cross-correlation method. The performed MART has used three projection angles of view in one plane (+60, 0, -90), 25 planes in z-direction, 100 rays in each projection angle, and capturing time of 1 second with the interval of 1/15000 second for the images. The intervals (+60 and -90) of the projection angle were not perfectly equivalent because of the space limitation and the shape of the nozzle.

If the intervals of the projection angles are not equivalent (e.g., +60° and -90°), more information can be obtained from the projection data than those of the equivalent case (e.g., +60° and -60°) because the projection directions are not symmetric each other.

Although the four-dimensional reconstruction has been carried out for all of the heights in z-direction simultaneously, Figures 4, 5 and 6 show the reconstructed density fields from 2, 10, 18 and 26 mm above the nozzle end with the time interval of 1/15000 sec because of the page limitation.

Before the initial flow at 8/15000 second, the density variation has been observed as shown in Fig. 4. The head of the helium flow released from the nozzle for 4/15000 sec after opening the solenoid valve has been reconstructed by the MART method from the speckle displacements. The head of the helium flow can occur by the delay of the solenoid valve or the rest of the helium in the nozzle from the previous experiment. The relative helium density in Figs.

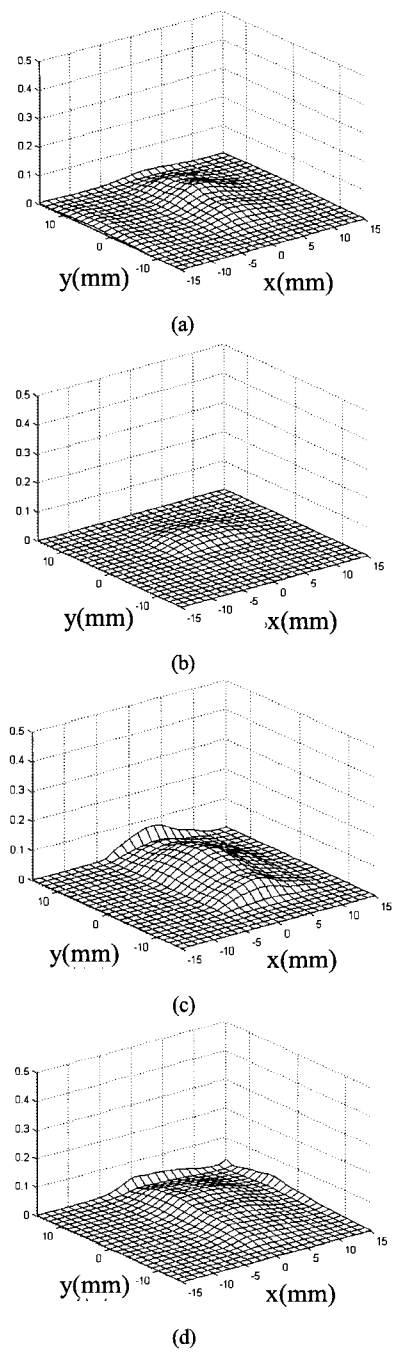

Fig. 4 Reconstructed fields at 4/15000 sec after opening valve by MART, (a) reconstructed field (Z = 2 mm), (b) reconstructed field (Z = 10 mm), (c) reconstructed field (Z = 18 mm), and (d) reconstructed field (Z = 26 mm)

4 and 5 can be calculated by Eq. (2) and the highest value of the helium density has been normalized to be 1 for 100 %. Although the reconstruction has been performed for the interval of 1/15000 sec after opening the valve, the results have been included for the cases of 8/15000, 9/15000 and 10/15000 second after opening the valve.

Figures 5 (a), (b), (c) and (d) show the density distributions for 2, 10, 18 and 26 mm from the nozzle end at 8/15000 second after starting the flow. The initial helium jet flow can be distinguished in the figures and the noises appear in the field because the amount of air in the mixture of air and helium is relatively large. Since the tomography has been carried out using three projection angles, the small errors can be observed near the measuring part. If the number of view increases, the noise can be reduced.

As the time passes, the density of the helium increases and the mixture with air decreases. Thus, the absolute value of the helium density increases and the less noise appear as shown by Figures 5 (e), (f), (g) and (h). For the case of 10/15000 second after opening the valve, the noises become relatively smaller because the helium flow is mixed less with air and is not affected by the surrounding air flow sensitively as shown in Figures 5 (i), (j), (k) and (l).

The high-speed helium density varies not only by the time change but also by the height change. Thus, the helium densities for 10 mm above the nozzle (Figures 5 (b), (f) and (j)) are lower than those for 2 mm from the nozzle end (Figures 5 (a), (e) and (i)) because the initial helium jetflow moves upward by the time. However, the densities for 18 mm above the nozzle (Figures 5 (c), (g) and (k)) do not show big discrepancies with those for 10 mm above the nozzle because the distance

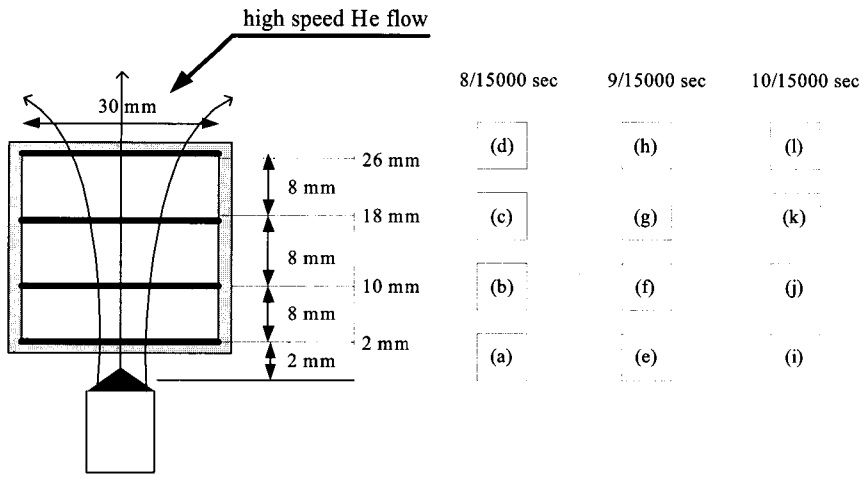

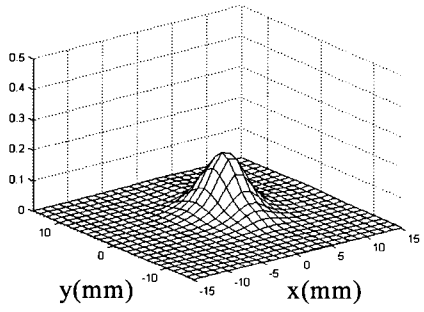

(a) 2 mm from nozzle for 8/15000 sec after opening

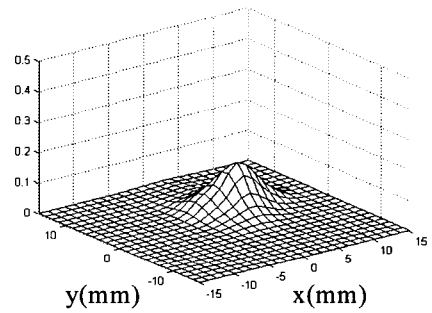

(b) 10mm from nozzle for 8/15000 sec after opening

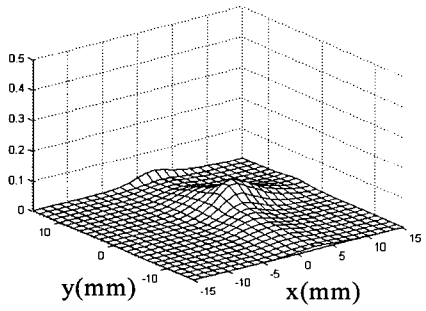

(d) 26mm from nozzle for 8/15000 sec after opening

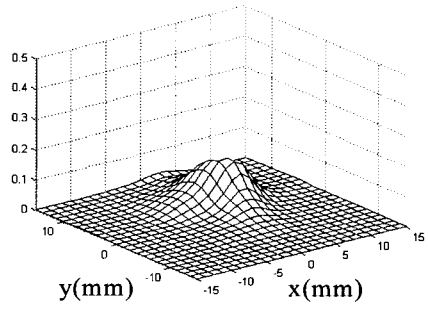

(c) 18mm from nozzle for 8/15000 sec after opening

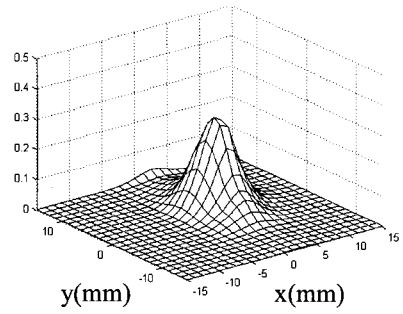

(e) 2mm from nozzle for 9/15000 sec after opening

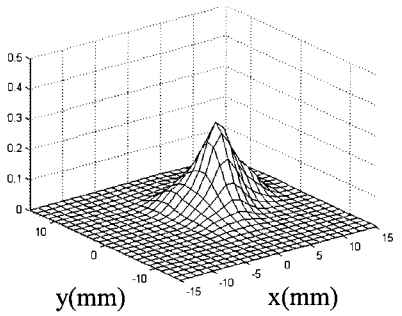

(f) 10mm from nozzle for 9/15000 sec after opening

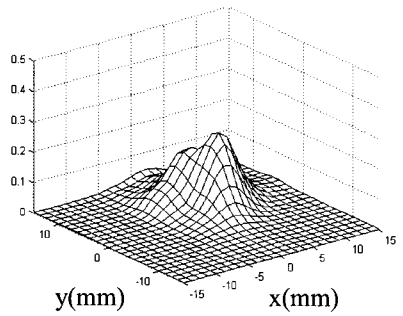

(g) 18mm from nozzle for 9/15000 sec after opening

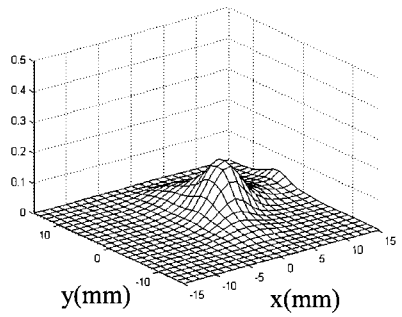

(h) 26mm from nozzle for 9/15000 sec after opening

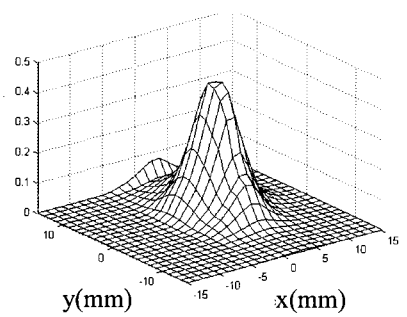

(i) 2mm from nozzle for 10/15000 sec after opening

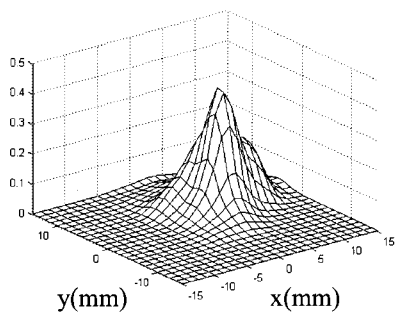

(j) 10mm from nozzle for 10/15000 sec after opening

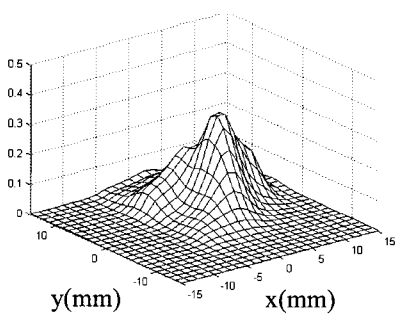

(k) 18mm from nozzle for 10/15000 sec after opening

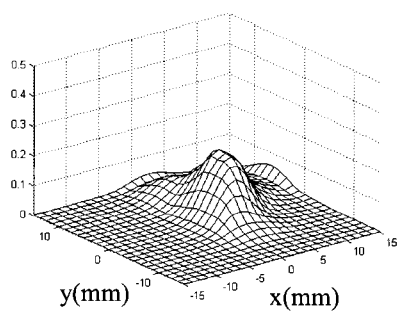

(l) 26mm from nozzle for 10/15000 sec after opening

Fig. 5 Reconstructed unsteady and three-dimensional density distributions of asymmetric and high-speed helium jet flow from triangular nozzle

from the nozzle and the effect of the noises are already large for those relatively low densities. Also, the helium densities for 26 mm from the nozzle end show very low values since the flow does not reach the point yet for such a short time.

The density variation with time at 18 mm above the nozzle end for the center of the nozzle surface has been drawn in Fig. 6 since the simultaneous four-dimensional reconstruction has been performed with time. As shown in Fig. 6, the density increases at 4/15000 second after opening the valve, which has been considered to be the density wave for the head of the helium jet flow. Then, the initial helium jet flow has appeared at 8/15000 second after the density had decreased. The increase of the density values after the initial helium jet flow can be confirmed in Fig. 6.

The calculation of the tomography has been performed in IBM PC with the P4-3.0 GHz and the RAM of 1 Gbyte and the average calculation time was 3 minutes 30 seconds for one instantaneous reconstruction. If the number of the iteration increases more than the optimum value, the profile of the density distribution includes more noises. Thus, the iteration has been stopped at the point for the accurate reconstruction. The developed digital speckle tomography can be used for the simultaneous four-dimensional density reconstructions of various high-speed gas flows in order to detect the real-time gas variation.

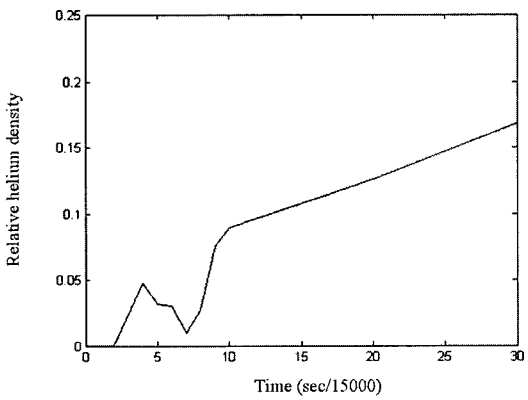

Fig. 6 Density variation of asymmetric and high-speed helium jet flow with time for 18mm above triangular nozzle at center location

7. Conclusion

The four-dimensional density distribution of the high-speed helium jet flow has been reconstructed by the developed real-time digital speckle tomography using three high-speed CCD cameras in this study instead of reconstructing two-dimensional distribution. The unsteady and initial helium jet flow at turbulent region has been analyzed so that the reconstruction can be applied for many engineering fields such as fuel injection, turbo machine, shock wave, etc. The noise in the reconstruction has appeared because the ambient air is unstable for a short time and the deflection angles from the speckle displacements have been integrated numerically for the interferometric fringe shifts. The limited number of the projection angles can also produce the noise because the laser rays of the projection angles cannot cover the whole reconstructed field in the experiment. The noises could be caused by the small vibration of the camera and the unstable surrounding air. However, the four-dimensional MART which has been confirmed in the numerical study has reconstructed the asymmetric and transient density distributions of the high-speed and initial helium jet flow with acceptable accuracies. This study can be applied for the inspection of the fast

hydrogen gas movement and the accurate analysis of various thermal flows.

Acknowledgement

This work was supported by the Korea Research Foundation Grant funded by the Korean Government (No. R08-2003-000-10030-0).

References

1) D. Schmidt, U. Krause, U. Schmidtchen, "Numerical simulation of hydrogen gas releases between buildings", Int. J. Hydrogen Energy, Vol. 24, 1999, pp. 479-488.
2) M. Françon M, "Laser Speckle and Applications in Optics", Academic Press, New York, 1979, pp. 64-103.
3) J. R. Partington, "Physico-Chemical Optics", Vol. IV, An Advanced Treatise on Physical Chemistry, Longmans Green, London, 1953, pp. 27-31.
4) K. D. Kihm, J. H. Kim, and L. S. Fletcher, "Investigation of Natural Convection Heat Transfer in Converging Channel Flows Using a Specklegram Technique", Journal of Heat Transfer Vol. 115, 1993, pp. 140-148.
5) T. C. Liu, W. Merzkirch, and K. Oberste-Lehn K, "Optical Tomography Applied to a Speckle Photographic Measurement of Asymmetric Flows with Variable Density", Exper Fluids, Vol. 7, 1989, pp. 157-163.
6) N. A. Fomin, "Speckle Photography for Fluid Mechanics Measurements", Springer, Berlin, 1998, pp. 105-146.
7) R. Gordon, "A Tutorial on ART", IEEE Trans. on Nuclear Science, Vol. NS-21, 1974, pp. 78-92.
8) D. Verhoeven, "Limited-data Computed Tomography Algorithms for the Physical Sciences", Appl. Opt., Vol. 32, No. 20, 1993, pp. 3736-3754.
9) H. S. Ko and K. D. Kihm, "An Extended Algebraic Reconstruction Technique (ART) for Density-Gradient Projections : Laser Speckle Photographic Tomography", Exper. Fluids, Vol. 27, No. 6, 1999, pp. 542-550.
10) M. Raffel, C. E. Willert, and J. Kompenhans, "Particle Image Velocimetry", Springer, Berlin, 1998, pp. 203-346.
11) K. M. Hanson and G. W. Wecksung, "Local Basis Function Approach to Computed Tomography", Appl. Opt., Vol. 24, No. 23, 1985, pp. 4028-4039.
12) H. S. Ko, K. Okamoto, and H. Madarame, "Reconstruction of Transient Three-dimensional Density Distributions Using Digital Speckle Tomography", Meas. Sci. Tech., Vol. 12, No. 8, 2001, pp. 1219-1226.
13) H. S. Ko and Y. -J. Kim, "Tomographic Reconstruction of Two-phase flows", KSME Int J Vol. 17, 2003, pp. 571-580.